Noncovalent Interaction between Single-Walled Carbon Nanotubes and Pyrene-Functionalized Gold Nanoparticles in Water-Soluble Nanohybrids

ARTICLE *in* THE JOURNAL OF PHYSICAL CHEMISTRY C · JANUARY 2014

Impact Factor: 4.77 · DOI: 10.1021/jp505005e

THE JOURNAL OF PHYSICAL CHEMISTRY C

Article

pubs.acs.org/JPCC

Noncovalent Interaction between Single-Walled Carbon Nanotubes and Pyrene-Functionalized Gold Nanoparticles in Water-Soluble Nanohybrids

Patrizio Salice,[†] Alessandro Gambarin,[†] Nicola Daldosso,[‡] Fabrizio Mancin,*[,†] and Enzo Menna*[,†]

[†]Dipartimento di Scienze Chimiche, Università di Padova, via Marzolo 1, 35131 Padova, Italy

[‡]Dipartimento di Informatica, Università degli Studi di Verona, strada le Grazie 15, 37134 Verona, Italy

ABSTRACT: The combination of different nanostructures in a multifunctional nanostructured hybrid is expected to improve their functionalities and lead to synergistic effects. In these regards, carbon nanotubes and gold colloids are well-studied building blocks with unique optical and electronic properties, which could be combined in a variety of optoelectronic applications. In this framework, we herein present an innovative approach to the preparation of water-soluble nanohybrids by noncovalent interaction between single-walled carbon nanotubes (SWCNTs) and gold nanoparticles (AuNPs) cofunctionalized with pyrenyl and choline residues. To this aim, we developed a procedure based on consecutive centrifugation steps, which allows straightforward isolation of the conjugates in their water-soluble form. Each step of the process was monitored by TEM and by UV−vis−NIR absorption spectroscopy to characterize the obtained nanohybrids and to confirm that the interaction of the pyrene residues of the cofunctionalized AuNPs with the nanotube walls is the only one responsible for the formation of the water-soluble nanohybrids. Further investigations including Raman spectroscopy and photoluminescence mapping confirm that the interaction between the AuNPs and the SWCNTs is arguably noncovalent and thus assures that the emission in the NIR region by the nanotubes is preserved. Measurements of the quenching of the fluorescence of pyrene by carbon nanotubes provide the association constants for complex formation between the cofunctionalized AuNPs and SWCNTs. The results reported herein provide the basis to novel strategies for the preparation of water-soluble nanohybrids between AuNPs and SWCNTs based on noncovalent interactions.

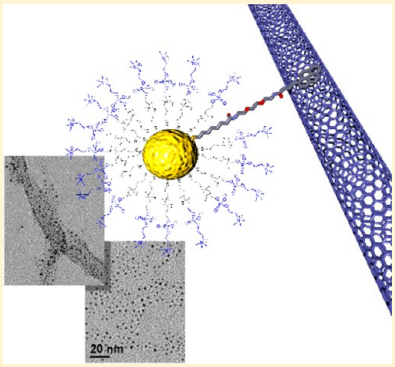

INTRODUCTION

Within the rich and assorted world of nanostructures, it is often convenient to combine the complementary properties of different systems to prepare hybrids with improved functionalities and synergistic effects. In particular, self-organization of nanosystems through programmed noncovalent interactions offers the possibility to produce complex and multifunctional structures. Among the others, gold colloids and carbon nanotubes (CNTs) are ideal building blocks since they both have peculiar and well-known properties arising from their nanosized dimensions.

Gold nanoparticles (AuNPs) covalently protected with a monolayer of thiols have tunable absorption and emission properties in the visible and NIR region, respectively.[1] The amplitude of their band gap depends on the size (1−500 nm) and the geometry (spherical, faceted, rod-like) of the nanoparticle, and their high oxidation potential (+0.9 V vs Ag/AgCl) reflects their excellent stability. In virtue of these properties, functionalized AuNPs are employed as sensors,[2] oxide-supported catalysts,[3] bioanalytes,[4] and optical components.[5] Moreover, their multifunctional nature enables the virtually endless possibility of introduction of functional groups in the monolayer, which can be exploited for several applications.[6−10] On the other hand, CNTs are made by sp^2-hybridized carbon atoms arranged in cylinders with diameter between 1 nm for single-walled CNTs (SWCNTs) and tens of nanometers for multiwalled CNTs (MWCNTs). Their length varies from hundreds of nanometers to millimeters. CNTs absorb through the UV, visible, and NIR region and are weak emitters in the NIR region (800−1400 nm). Indeed, they possess metallic or semiconducting character with size-dependent band gaps below 1 eV and low oxidation potential (+0.4−0.5 V vs Ag/AgCl), which set both their valence and conduction bands in the middle of the AuNP band gap. They have good thermal and electrical conductivities, which have been largely exploited in a wide range of applications[11] including sensing,[12] photovoltaics and photodetection,[13,14] biomedical applications,[15] batteries and supercapacitors,[16] heterogeneous catalysis,[17] and field emission.[18]

Under this perspective, the hybrids resulting from the interaction of the external walls of CNTs with AuNPs, hereafter referred to as SWCNT−AuNP, could find several applications in sensing, catalysis, and photoelectronic materials to cite a few.

These envisioned outcomes have already led to the preparation of different assortments of CNT−AuNP nanohybrids, for example, by direct formation of gold colloids

Received: May 21, 2014
Revised: July 31, 2014
Published: September 16, 2014

   dx.doi.org/10.1021/jp505005e | J. Phys. Chem. C 2014, 118, 27028−27038

Scheme 1. Schematic Representation of the Nanostructures Used: Cofunctionalized AuNP-*x*% (*x* Refers to the Percentage of Pyrene Residues (8) in the Monolayer), AuNP-0%, Pristine SWCNT, and SWCNT-PEG

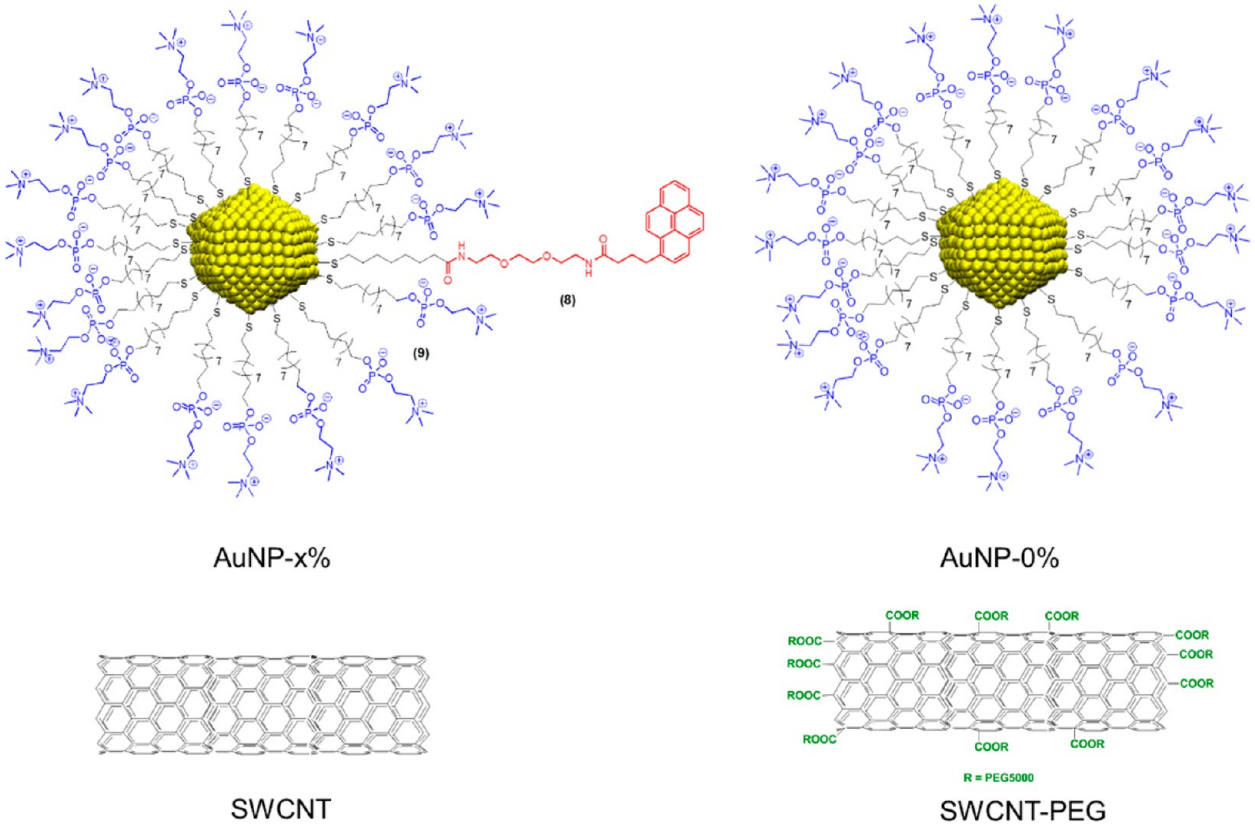

following electrochemical reduction of gold precursors in the presence of CNTs.[19] While this procedure affords a noncontinuous assembly of gold clusters on the surface of SWCNTs, it lacks a tight control on the dimension of the gold colloids. An alternative to this method is based on the growth of AuNPs in the presence of CNTs covalently functionalized with thiols.[20] The thiols provide the necessary protective group around which the gold colloids grow during the in situ reduction of $HAuCl_4$ by a metal hydride.[20] More versatile methods rely on the interaction between preformed AuNPs and pristine CNTs, by either covalent or noncovalent interactions. In both cases, the dispersity and mean diameter of the gold colloids could be determined a priori by a suitable choice of the synthetic methodology. Moreover, several reported procedures consider also the use of untreated commercial CNTs. In this regard, a successful covalent approach is based on a cyclopropanation reaction between pristine MWCNTs and AuNPs with diameter in the range 1.8−3.9 nm and protected by a bifunctional thiol bearing a diaziridine.[21]

Noncovalent procedures bring about the advantage to allow self-organization of systems of higher complexity. Moreover, self-organized systems can be easily modified or optimized by the simple substitution of the building blocks. In the case of CNTs, a reliable approach can be based on the prominent interaction established between a pyrene moiety and the CNT.[22] Recently, CNTs have been functionalized noncovalently with pyrene derivatives of nickel complexes to obtain electrocatalytic materials for hydrogen uptake and evolution,[23] of polyhedral oligomeric silsesquioxanes for electrostatic discharge membranes,[24] and of biotin for biosensing.[25] Also pyrene derivatives functionalized with thiols were employed to bind AuNPs to preformed pyrene−CNT conjugates.[26] In this notable example, a dispersion of MWCNTs covalently functionalized with didecylamine was sonicated, filtered, and washed in the presence of 17-(1-pyrenyl)-13-oxo-heptadecanethiol obtaining a conjugate where the pyrene derivatives noncovalently attached to the walls of CNT exposed thiol groups. Addition of a gold colloid to this dispersion resulted in a complex mixture of MWCNTs and AuNPs linked to the nanotubes through the pyrenyl linker. Characterization of this system by TEM and fluorescence, UV−vis−NIR, and Raman spectroscopies induced the authors to conclude that charge transfer interactions between CNTs and AuNPs may occur in noncovalent nanohybrids, but the control on system composition is hardly achieved.

This issue may be overcome by using multifunctional monolayer-protected AuNPs instead of gold colloids in dispersion. Indeed, the synthesis of AuNPs cofunctionalized with water-soluble choline residues and pyrenyl derivatives (Scheme 1) is expected to lead to a better control on the composition and the features of the obtained hybrid. In this article, we describe the synthesis of multifunctional AuNPs with a variable percentage of pyrenyl derivatives on their protecting monolayer, and we demonstrate how it is possible to monitor and to control the strength of the interaction between AuNPs and SWCNTs to spontaneously obtain water-soluble nanohybrids.

EXPERIMENTAL SECTION

Materials and Methods. Dichloromethane (DCM), diisopropylethylamine (DIPEA), *N*-(3-(dimethylamino)-

dx.doi.org/10.1021/jp505005e | J. Phys. Chem. C 2014, 118, 27028−27038

Scheme 2. Synthesis of Pyr-SH (8)

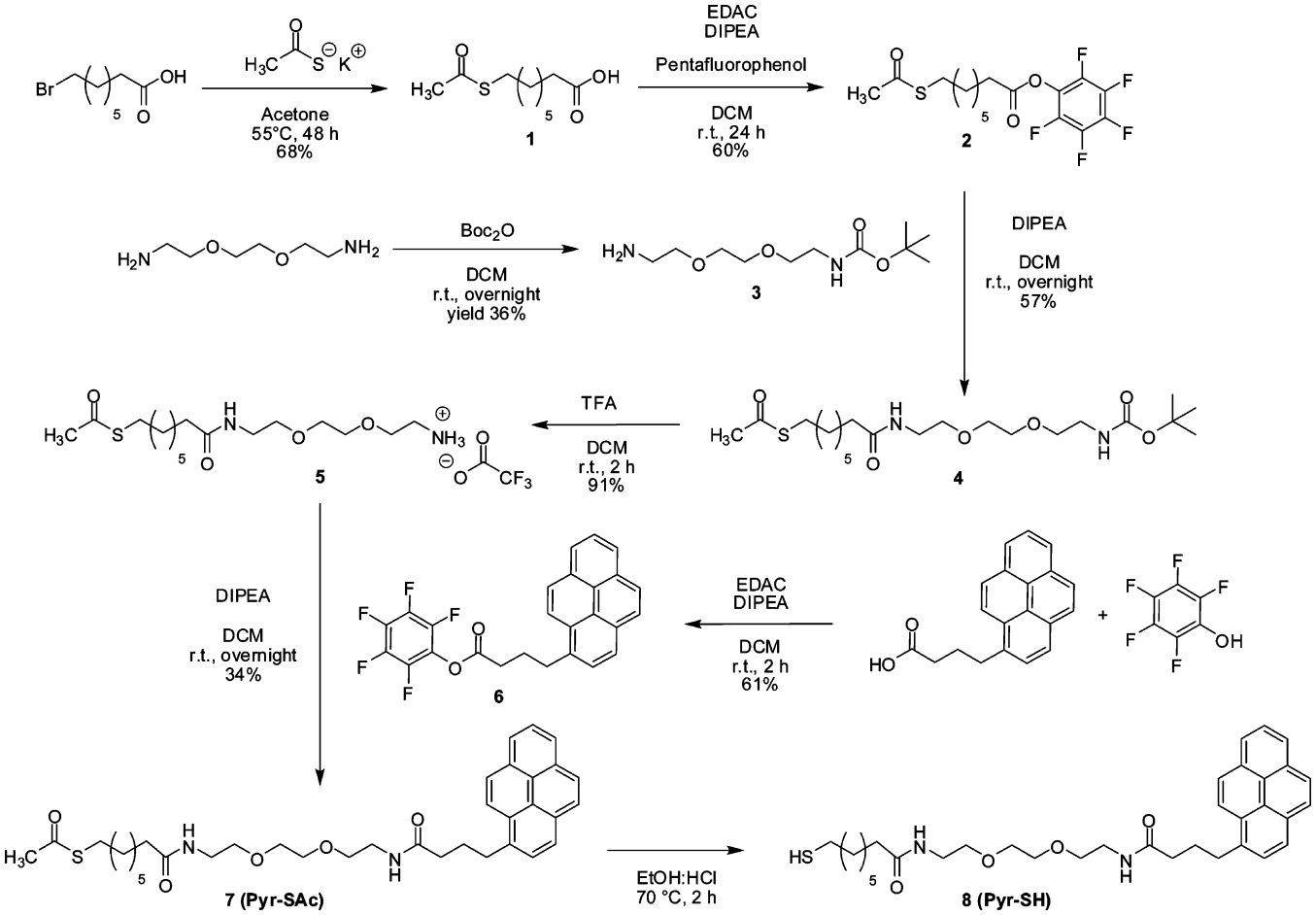

propyl)-*N*′-ethylcarbodiimide hydrochloride (EDAC), trifluoroacetic acid (TFA), dimethylformamide (DMF), tetraoctylammonium bromide (TOABr), and all the other reagents and solvents used were purchased from Sigma-Aldrich and were used as received if not otherwise specified. SWCNTs (HiPCO, CNI lot# P2150, diameter 0.85−1.15 nm) were purchased from Carbon Nanotechnologies, Inc. (CNI, batch number P2150) and were used as received. 12-Mercaptododecyl (2-(trimethylammonio)ethyl) phosphate[27] (thiol **9**) and AuNPs[28] were synthesized according to reported procedures. All aqueous solutions were prepared using Milli-Q water with >18 MΩ cm resistivity.

TLC analyses were performed using Merck 60 F_{254} precoated silica gel glass plates. Column chromatography was carried out on Macherey-Nagel silica gel 60 (70−230 mesh). NMR spectra were recorded on a Bruker Avance (250 MHz ^{1}H frequency, 62.9 MHz ^{13}C frequency). Chemical shifts are reported relative to internal Me_4Si. Multiplicity is given as follows: s = singlet, d = doublet, t = triplet, q = quartet, qn = quintet, m = multiplet, b = broad peak. ESI-MS mass spectra were obtained with an Agilent Technologies LC/MSD Trap SL mass spectrometer.

UV−vis absorption spectra are recorded with a UV−vis−NIR Cary 5000 spectrophotometer (Agilent Technologies, Inc., room temperature, spectral range 280−1400 nm, data interval = 0.5 nm, scan rate = 300 nm/min, SBW = 2 nm). Steady-state UV−vis−NIR fluorescence spectroscopy is carried out using both an LS 55 fluorescence spectrophotometer (PerkinElmer, Inc.) to study the emission properties of pyrene between 300 and 700 nm and a Jobin Yvon NanoLog spectrofluorometer (HORIBA Scientific, Ltd.) to measure photoluminescence excitation maps of SWCNTs in the NIR region. A portion of the aqueous solution of each SWCNT−AuNP nanohybrid was drop-cast on precleaned glass microslides (Corning) and annealed at 110 °C. The resulting thin film was characterized with an Invia Renishaw Raman microspectrometer (50× objective) using the 633 nm line of a He−Ne laser at room temperature with a low laser power. Analogously, a portion of the SWCNT−AuNP solution was drop-cast on silicon and was then observed with a JEOL 3010 transmission electron microscope operated at 300 kV at various magnifications.

*Synthesis of 8-(Acetylthio) Octanoic Acid (**1**).* An amount of 2.89 g (13.0 mmol) of 8-bromooctanoic acid is dissolved in 60 mL of acetone, and 1.95 g (17.1 mmol) of potassium thioacetate are added. The reaction is refluxed for 48 h (monitored by TLC, DCM:MeOH, 9.5:0.5, R_f = 0.5). The solvent is then evaporated; the solid obtained is dissolved in DCM; and the resulting solution is extracted with water (3 × 30 mL) and dried with Na_2SO_4. After evaporation of the solvent, 1.93 g of product (68.0%) is obtained. ^{1}H NMR (250 MHz, $CDCl_3$) δ: 2.84 (t, 7.2 Hz, 2H, CH_2S); 2.34 (m, 5H, CH_2CO, CH_3); 1.56 (bm, 4H, aliphatic chain); 1.33 (bm, 6H, aliphatic chain).

*Synthesis of Perfluorophenyl 8-(Acetylthio) Octanoate (**2**).* Amounts of 1.93 g (8.8 mmol) of **1**, 2.0 mL of DIPEA (11.5 mmol), and 2.20 g (11.5 mmol) of EDAC are dissolved in 50 mL of DCM. The reaction flask is placed into a 0 °C ice bath,

dx.doi.org/10.1021/jp505005e | J. Phys. Chem. C 2014, 118, 27028−27038

and a solution of pentafluorophenol (2.11 g, 11.5 mmol) in DCM (10 mL) is added dropwise. The reaction is allowed to proceed at RT for 24 h (monitored by TLC, DCM:petroleum ether, 1:1, R_f = 0.8). The solvent is then evaporated, and the residue is purified by flash chromatography (silica gel, DCM:petroleum ether, 1:1), to obtain 2.4 g (59.9%) of product. ^{1}H NMR (250 MHz, $CDCl_3$) δ: 2.87 (t, 7.2 Hz, 2H, CH_2S); 2.64 (t, 7.6 Hz, 2H, CH_2CO); 2.29 (s, 3H, CH_3); 1.75 + 1.56 + 1.36 (bm, 10H, aliphatic chain).

*Synthesis of tert-Butyl (2-(2-(2-Aminoethoxy)ethoxy)-ethyl)carbamate (**3**).* An amount of 10 mL (66.8 mmol) of 2,2′-(ethylenedioxy)bisethylamine is dissolved in 10 mL of dioxane, and 2.43 g (11.1 mmol) of di-*tert*-butyl dicarbonate dissolved in 10 mL of dioxane is then added dropwise to the solution. The reaction mixture was allowed to react at RT overnight (monitored by TLC, DCM:MeOH:NH_3, 10:1:0.1, R_f = 0.4, detection with ninhydrin spray). After evaporation of the solvent, the residue is dissolved in DCM, and the solution is extracted with water (3 × 30 mL), dried with Na_2SO_4, and evaporated to obtain 1.0 g (36.3%) of product. ^{1}H NMR (250 MHz, $CDCl_3$) δ: 5.19 (bt, 1H, NH); 3.49 (m, 6H, $NH_2CH_2CH_2OCH_2CH_2O$); 3.42 (t, 6.9 Hz, 2H, CH_2NH); 3.19 (bm, 2H, CH_2NH_2); 2.74 (t, 6.8 2H, CH_2CH_2NH); 1.62 (bs, 2H, NH_2); 1.31 (s, 9H, CH_3 Boc).

*Synthesis of 2,2-Dimethyl-4,15-dioxo-3,8,11-trioxa-5,14-diazadocosan-22-yl Ethanethioate (**4**).* Amounts of 703 mg (1.8 mmol) of **2** and 343 μL (2.0 mmol) of DIPEA are dissolved in 10 mL of DCM. The reaction mixture is brought to 0 °C in an ice bath, and 500 mg (2.0 mmol) of **3** is added dropwise. The reaction mixture is stirred at RT overnight and then extracted with water several times (monitored by TLC, ethyl acetate, R_f = 0.8). After removal of the solvent, the residue is purified by flash chromatography (silica gel, ethyl acetate) to obtain 464 mg (56.6%) of product. ^{1}H NMR (250 MHz, $CDCl_3$) δ: 1.26 (bm, 6H, CH_2 aliphatic chain); 1.40 (s, 9H, CH_3, Boc); 1.54 (m, 4H, CH_2CH_2CO + CH_2CH_2S); 2.13 (t, 7.5 Hz, 2H, CH_2CO aliphatic chain); 2.27 (s, 3H, CH_3); 2.77 (t, 6.9 Hz, 2H, CH_2NH TEG chain); 2.83 (m, 2H, CH_2S); 3.28 (m, 2H, CH_2NH TEG chain); 3.41 (t, 6.8 Hz, 4H, CH_2O TEG chain); 3.56 (bs, 4H, OCH_2CH_2O TEG chain).

*Synthesis of (8-((2-(2-(2-Aminoethoxy)ethoxy)ethyl)-amino)-8-oxooctyl) Ethanethioate Trifluoroacetic Salt (**5**).* An amount of 250 mg (0.6 mmol) of **4** is dissolved in 5 mL of DCM in a 10 mL round-bottom flask. TFA (3.0 mL) is then added and the reaction mixture is allowed to react at RT for 2 h. Solvent is finally removed by evaporation at reduced pressure to obtain 235 mg (yield = 91%) of product. ^{1}H NMR (250 MHz, $CDCl_3$) δ: 1.28 (bs, 6H, CH_2 aliphatic chain); 1.51 (m, 4H, CH_2CH_2CO + CH_2CH_2S); 2.31 (t, 7.6 Hz, 2H, CH_2CO); 2.32 (s, 3H, CH_3); 2.83 (t, 7.2 Hz, 2H, CH_2S); 3.23 + 3.59 + 3.72 (m, 12H, CH_2 TEG chain); 7.16 (bs, 1H, NH); 7.52 (bs, 2H, NH_3).

*Synthesis of Perfluorophenyl 4-(Pyren-1-yl) Butanoate (**6**).* Amounts of 288 mg (1.0 mmol) of 4-(pyren-1-yl) butanoic acid and 230 mg (1.2 mmol) of EDAC are dissolved in 30 mL of DCM. Then, 257 μL (1.5 mmol) of DIPEA is added, and the reaction mixture is cooled to 0 °C in an ice bath. A solution of pentafluorophenol (153 mg, 1.2 mmol) in DCM (10 mL) is then added dropwise, and the reaction mixture is allowed to react at RT overnight (monitored by TLC, $CHCl_3$, R_f = 0.8). The solvent is then removed by evaporation at reduced pressure, and the residue is purified by silica gel flash chromatography ($CHCl_3$), to obtain 274 mg (61%) of product. ^{1}H NMR (250 MHz, $CDCl_3$) δ: 1.71 (m, 2H, $PyrCH_2CH_2$); 2.23 (t, 7.6 Hz, 2H, CH_2CO); 3.06 (t, 7.2 Hz, 2H, $PyrCH_2$); 7.6−8.5 (m, 9H, CH, aromatic)

*Synthesis of S-(4,15-Dioxo-1-(pyren-1-yl)-8,11-dioxa-5,14-diazadocosan-22-yl) Ethanethioate (**7**, **Pyr-SAc**).* Amounts of 274 mg of **6** (0.6 mmol) and 235 mg of **5** (0.5 mmol) are dissolved in 20 mL of DCM, and the reaction mixture is stirred at RT overnight (monitored by TLC, $CHCl_3$:MeOH, 9.5:0.5, R_f = 0.2). The solvent is then removed by evaporation at reduced pressure, and the residue is purified by flash chromatography (silica gel, $CHCl_3$:MeOH, 9.5:0.5) to obtain 210 mg (34%) of product (**Pyr-SAc**). ^{1}H NMR (250 MHz, $CDCl_3$) δ: 1.23 (bs, 8H, CH_2 aliphatic chain + $PyrCH_2CH_2CH_2$); 1.51 (m, 4H, CH_2CH_2CO + CH_2CH_2S); 2.05 (t, 7.5 Hz, 2H, CH_2CO); 2.23 (t, 7.4 Hz, 2H, $PyrCH_2CH_2CH_2$); 2.30 (s, 3H, $SCOCH_3$); 2.49 (t, 7.3 H,$PyrCH_2$); 2.83 (t, 7.2 Hz, 2H, CH_2S); 3.2−3.7 (m, 12H, CH_2 TEG chain); 5.98 (bt, 1H, NH); 5.79 (bt, 1H, NH); 7.8−8.3 (m, 9H, CH, aromatic).

^{13}C NMR (62.9 MHz, $CDCl_3$) d: 173.8, 173.4, 172.7, 135.9, 131.4, 130.9, 128.7, 127.5, 127.4, 126.7, 125.9, 124.9, 124.8, 123.4, 70.2, 69.8, 60.4, 45.8, 39.3, 35.9, 32.8, 30.6, 29.7, 29.4, 29.0, 28.8, 27.5, 15.6, 14.8, 8.6.

ESI-MS (CH_3CN, m/z): 619.3 [20%, M + H^+], 641.2 [100%, M + Na^+], 657.0 [5%, M + K^+].

*Synthesis of 8-Mercapto-N-(2-(2-(2-(4-(pyren-1-yl)-butanamido)ethoxy)ethoxy)ethyl) Octanamide (**8**, **Pyr-SH**).* Compound **Pyr-SAc** is then dissolved, in the amount needed for nanoparticle coating in EtOH:HCl 6 M 1:1 and reacted at 70 °C for 2 h to provide deprotected product **Pyr-SH**.

^{1}H NMR (250 MHz, $CDCl_3$) δ: 1.28 (bs, 8H, CH_2 aliphatic chain + $PyrCH_2CH_2CH_2$); 1.44 (m, 4H, CH_2CH_2CO + CH_2CH_2S); 2.27 (t, 7.5 Hz, 2H, CH_2CO); 2.39 (t, 7. 2H, $PyrCH_2CH_2CH_2$); 2.55 (t, 2H, $PyrCH_2$); 2.79 (m, 2H, CH_2S); 3.30−3.53 (m, 12H, CH_2 TEG chain); 7.7−8.4 (m, 9H, CH, aromatic).

Preparation of AuNP. An amount of 100 mg (0.254 mmol) of $HAuCl_4 \times 3H_2O$, previously weighted under a N_2 atmosphere, is dissolved in 4 mL of Milli-Q water, obtaining a yellow solution. An amount of 5 g (9.14 mmol) of TOABr is dissolved into 250 mL of toluene (previously degassed). The Auric salt is then extracted from the aqueous solution into the toluene one by extraction with the organic phase divided into three aliquots. The aqueous solution gets colorless, and the organic one turns to a reddish color. The organic phase is transferred into a round-bottomed flask and vigorously stirred for 10 min under a nitrogen atmosphere, and then dioctylamine (4.2 mL, 13.94 mmol) is added under stirring. The solution becomes slowly colorless. After complete decoloring, 91.2 mg (2.44 mmol) of $NaBH_4$, dissolved in 4 mL of Milli-Q water, is quickly added under vigorous stirring. The solution immediately turns to black due to gold reduction. The reaction flask is left under stirring for 2 h, and then the water phase is removed using a separation funnel. Finally, a 2-propanol solution of the desired thiols (42% in moles with respect to the tetrachloaurate salt used) is added; in the case of mixed monolayer nanoparticles, a correction factor of 3 for the pyrenyl derivative **Pyr-SH** is used. Nanoparticle solution is then left under stirring overnight. Nanoparticles bearing phosphorylcholine derivatives (**9**) are purified by centrifugation in toluene (3 × 30 mL, 3500 rpm, 5 min) and subsequently by molecular exclusion chromatography (Sephadex LH-20, eluent: MeOH). Nanoparticles stabilized only by **Pyr-SH** are purified, after removal of

dx.doi.org/10.1021/jp505005e | J. Phys. Chem. C 2014, 118, 27028−27038

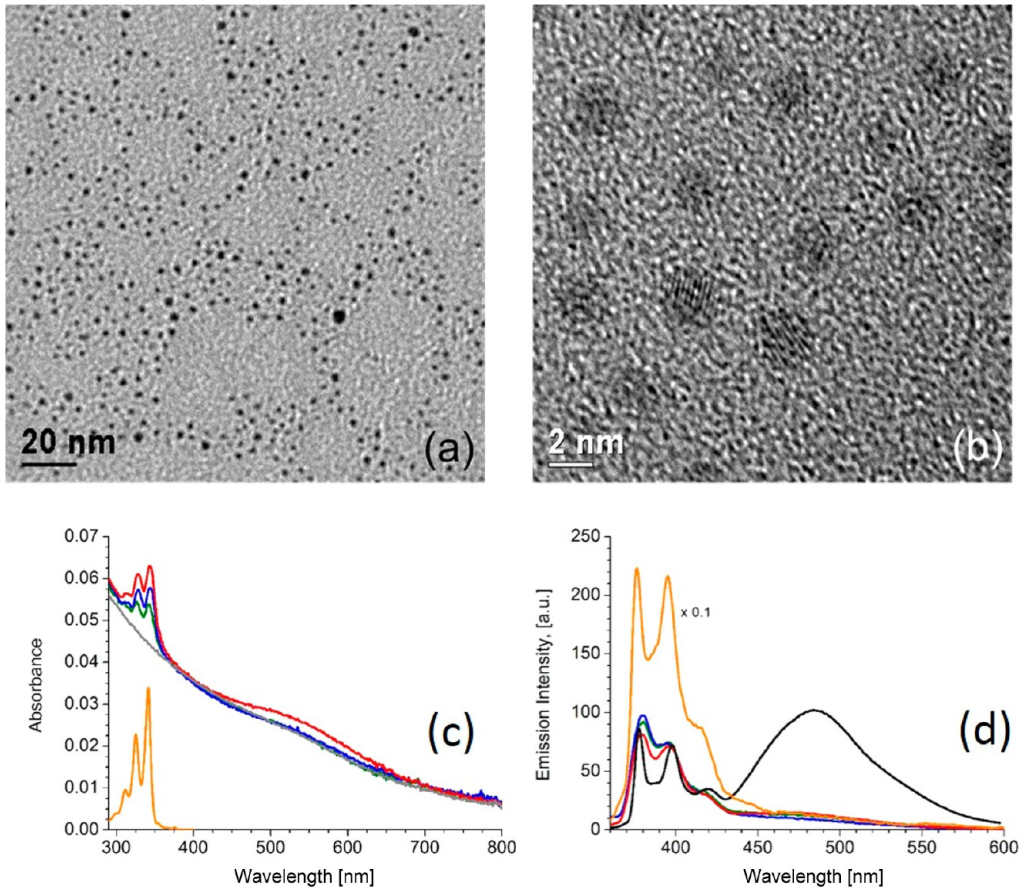

Figure 1. (a) and (b) TEM images of AuNP-0% acquired at 10 kV at different magnifications. (c) UV−vis spectra of AuNP-0% (gray), AuNP-5% (green), AuNP-10% (blue), AuNP-15% (red), and Pyr-SAc (orange) in methanol ([AuNP-*x*%] = 5 × 10^{-8} M, [Pyr-SAc] = 1 × 10^{-6} M). (d) Fluorescence emission spectra ([pyr] = 1 × 10^{-6} M, λ_{exc} = 345 nm) of Pyr-SAc (orange, rescaled), AuNP-5% (green), AuNP-10% (blue), AuNP-15% (red), and AuNP-100% (black) in methanol.

the organic solvent (toluene) by evaporation at reduced pressure, through several cycles of molecular exclusion chromatography (Sephadex X1, eluent: CH_2Cl_2).

^{1}H NMR (250 MHz, CD_3OD, AuNP-0%) δ: 1.2−1.4 (bs, CH_2 aliphatic chain); 1.68 (bs, $CH_2CH_2CH_2O$); 3.28 (bs, $N(CH_3)_3$); 3.72 (bs, $CH_2CH_2CH_2O$); 3.90 (bs, OCH_2CH_2N); 4.30 (bs, OCH_2CH_2N). ^{1}H NMR (250 MHz, $CDCl_3$, AuNP-100%) δ: 1.2−1.3 (bs, CH_2 aliphatic chain); 1.83 (bs, $CH_2CH_2CH_2Pyr$ + $CH_2CH_2C{=}O$); 2.0−2.2 (bm, CH_2Pyr, $PyrCH_2CH_2CH_2$ $CH_2C{=}O$); 3.2−3.5 (bs, CH_2O + CH_2N); 7.7−8.2 (bm, aromatic). Composition of AuNP-5%−15% was determined by integration of distinctive signals of **Pyr-SH** and PC-SH after thiol detachment with I_2 in deuterated methanol.

Preparation of the SWCNT−AuNP Nanohybrids. Amounts of 0.1 mg of SWCNTs are added to a solution of AuNP-*x*% (gold nanoparticles with *x*% of pyrene loading, where *x* is 0, 5, 10, 15, and 100) in 5.0 mL of Milli-Q water. The resulting suspension is sonicated until the SWCNTs are finely dispersed (Tip sonicator Misonix 3000, power: 1 W/mL, pulse on: 3 s, pulse off: 3 s, sonication time: 5 min). This suspension is centrifuged at 4000 rpm for 5 min (IEC CL10 centrifuge, Thermo Corporation) to remove the SWCNTs not bound to the AuNPs (hence insoluble in water). Indeed, while the supernatant contains both free AuNPs and the complex SWCNT−AuNP, the unbound CNTs are collected at the bottom of the glass centrifugation tube. After three centrifugation cycles, the supernatant is free from unbound CNTs. Then, the supernatants are loaded in Nalgene centrifuge tubes (Oak Ridge Style 3119) and are subsequently centrifuged at 12 500 rpm for 60 min (MR23i ultracentrifuge, Thermo Fisher Scientific, Inc.) to remove the free AuNPs. In this case, the supernatant contains only free AuNP, while the complex SWCNT−AuNP is collected at the bottom of the PTFE centrifugation tube. After 4 centrifugation cycles the supernatant is free from unbound AuNPs. The black residue collected at the bottom of the tube is redissolved in 7 mL of Milli-Q water and is characterized as indicated previously.

RESULTS AND DISCUSSION

Synthesis of Cofunctionalized Water-Soluble AuNPs. Thiols **Pyr-SH** (Scheme 2) and **9** were selected as candidates to prepare mixed monolayer-coated gold nanoparticles with 2 nm gold core diameter.[29] Thiol **9**, bearing a phosphorylcholine headgroup, ensures good solubility to the nanoparticles in water and even saline solutions, a property desirable for both biological applications and the development of eco-friendly procedures for processing AuNPs not requiring organic solvents. On the other hand, thiol **Pyr-SH**, bearing the pyrene moiety, should give nanoparticles the ability to interact with the CNT surface.

The two thiols were used in the synthesis of the cofunctionalized AuNPs using a two-step procedure. Accordingly, in the first step the nanoparticles are formed by reduction of $AuCl_4^-$ with aqueous $NABH_4$ in a two-phase (water/

dx.doi.org/10.1021/jp505005e | J. Phys. Chem. C 2014, 118, 27028−27038

toluene) system in the presence of dioctylamine as a weak stabilizer and tetraoctylammonium chloride as a phase-transfer catalyst.[30] In the second step, a stoichiometric amount of the two thiols is added to form the final monolayer by thiol/amine substitution at the gold surface. One advantage of this method is the ability to obtain quite monodisperse AuNP samples as confirmed by the TEM images of AuNP-0% reported in Figure 1a and b, which show that the gold core of AuNPs has a diameter of (2.7 ± 1.0) nm. DLS measurements on aqueous solution of AuNP-0% (not shown) are in agreement with this value, too. The low polydispersity and the good solubility in water (for nanoparticles with a coating mainly composed of **9**), alcohols, DMF, and DMSO are altogether favorable properties in the preparation of SWCNT-based nanohybrids.

Moreover, the two-step procedure enables the use of lower amounts of thiols for the monolayer formation and, on theory, a better control of molecular composition in the case of mixed monolayers.[28] Given these considerations, we prepared five different batches of AuNPs cofunctionalized with the choline derivative **9** and the pyrenyl moiety **Pyr-SH**: AuNP-0%, AuNP-5%, AuNP-10%, AuNP-15%, and AuNP-100%. These samples differ by the percentage of the pyrenyl residues in the monolayer. Monolayer composition was determined by ^{1}H NMR spectroscopy by integration of **9** and **Pyr-SH** distinctive signals after nanoparticle decomposition with I_2. In general, we found that the monolayer contains a percentage of pyrenyl residue **Pyr-SH** smaller than that of the coating mixture. Since the general average formula for these nanoparticles is $Au_{678}RS_{134}$,[31] the number of pyrenyl residues per nanoparticle in the series is, respectively, 0, 7, 13, 20, and 134.

UV−vis absorption and emission spectroscopies showed that the distinctive features of the pyrene unit have been preserved after the functionalization procedure. In Figure 1c we report the absorption spectra of AuNPs with different loading of pyrene in methanol, which is a good solvent for both hydrophilic AuNP-0%, AuNP-5%, AuNP-10%, and AuNP-15% and hydrophobic AuNP-100%. As expected, a higher amount of **Pyr-SH** on the protecting monolayer results in an increase in the absorption intensities of the pyrene monomer with respect to the absorption of gold nanoparticles (see the spectrum of AuNP-0%). Indeed, the presence of a small shoulder at 520 nm in the UV−vis spectra of the nanoparticles (Figure 1c) is in agreement with the size of the gold core determined by TEM since strong surface plasmon resonance (SPR) bands are expected only for gold nanoparticles larger than 3 nm. The emission spectra of AuNP-5%, -10%, and -15% in methanol reported in Figure 1d are consistent with the emission of monomeric pyrene species and thus suggest that the pyrene moieties in the protecting monolayer are not interacting with each other.[32,33] On the other end, AuNP-100% exhibits the emission of an excimer species arguably due to the confinement of pyrene moieties next to each other at this loading.

Quenching of the Fluorescence of Pyrene-Functionalized AuNPs by SWCNTs. The formation of noncovalent bonds between pyrene derivatives and CNTs has been widely exploited in the preparation of multifunctional nanoassemblies,[34−36] and therefore different methods have been developed to probe this interaction. In particular, the determination of the association constant for complex formation from fluorescence measurements[26,37] requires small amounts of material in solution and thus fits the scale adopted for the synthesis of SWCNT−AuNP nanohybrids. Indeed, the addition of a dispersion of SWCNTs to a solution of cofunctionalized AuNPs is expected to produce the quenching of the emission of pyrenyl moieties due to the interaction with the SWCNT walls to form nonfluorescent complexes.

Pyrenyl-functionalized water-soluble nanoparticles could act as transporters of SWCNTs in aqueous solutions. For this reason, we initially investigated the interaction between AuNPs and SWCNTs in water using AuNP-5%, AuNP-10%, and AuNP-15% and a water-soluble SWCNT derivative bearing polyethylene glycol (PEG) chains (SWCNT-PEG, see Scheme 1, PEG molecular weight: 5000 g/mol).[38,39] However, when increasing amounts of SWCNT-PEG were added to aqueous solutions of AuNP-5%, AuNP-10%, and AuNP-15% no decrease of the pyrene emission was detected after correction for dilution and inner filter effect of the SWCNTs.

To obtain more insight on this behavior we repeated the experiment with DMF as a solvent, thus enabling us to study also pristine nanotubes and AuNP-100%. Acetylthiol **Pyr-SAc** was first investigated as a benchmark to study the interaction of the pyrenyl moiety with SWCNTs. Upon addition of a dispersion of pristine SWCNTs to a solution of **Pyr-SAc**, both in DMF, we observed a significant emission quenching, which confirms that pyrene binds to SWCNT walls also in DMF (Figure 2). Quenching of pyrene emission is however not

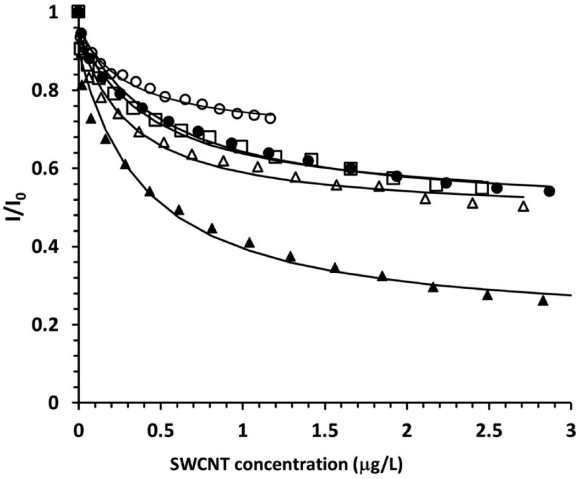

Figure 2. Quenching of **Pyr-SAc** (7, open circles), AuNP-5% (open squares), AuNP-10% (filled circles), AuNP-15% (open triangles), and AuNP-100% (filled triangles) emission (λ_{exc} = 345 nm, λ_{em} = 381 nm) by pristine SWCNTs in DMF.

complete, indicating that the molecule is still partially emissive once adsorbed on the CNT walls. Also in the case of AuNP-5%, AuNP-10%, AuNP-15%, and AuNP-100%, the addition of pristine SWCNTs led to a substantial quenching of the pyrene emission (Figure 2). On the other, no emission decrease was observed upon addition of SWCNT-PEG, confirming that the CNT functionalization prevents the interaction between the nanoparticles and the nanotube walls because of the larger steric encumbrance of PEG. Emission intensity versus pristine SWCNT concentration profiles could be fitted, for both **Pyr-SAc** and AuNPs, with a 1:1 binding model that takes into account the emission of both the bound and unbound pyrene.

The fitting results for **Pyr-SAc**, AuNP-5%, AuNP-10%, AuNP-15%, and AuNP-100% are reported in Table 1.

Interestingly, the affinities of nanoparticles for pristine SWCNTs are similar to that of the pyrenyl derivative **Pyr-SAc**, and they even show a slight decrease with increasing

dx.doi.org/10.1021/jp505005e | J. Phys. Chem. C 2014, 118, 27028−27038

Table 1. Association Constant for Complex Formation (K_a) and Fraction of Pyrene Emission Intensity Decrease upon Binding to Pristine SWCNTs

	K_a[a]	Quenching (%)
PyrSAc (7)	4.0 ± 0.8	28.5
AuNP-5%	3.3 ± 0.6	49.2
AuNP-10%	2.2 ± 0.3	49.3
AuNP-15%	2.3 ± 0.4	46.9
AuNP-100%	2.5 ± 0.5	78.7

[a]Reported as × 10^6 mL/mg.

pyrene loading. Apparently, such figures indicate that the cooperation between multiple pyrene units on the same particle in binding the SWCNT walls is hampered. The decreasing trend in K_a values indicates that such an effect arises neither from the small number of pyrene units present on the surface of nanoparticles nor from the unfavorable interaction between the hydrophobic surface of SWCNTs and the polar phosphorylcholine groups on the nanoparticles. More likely, such decreasing affinity arises from the self-aggregation of pyrene units, which should be more relevant at higher loading and would decrease their availability for binding to nanotubes, from the folding of the pyrenyl moieties inside the hydrophobic monolayer or from the high surface curvature of these small nanoparticles, which could limit the number of suitably oriented pyrene groups on each AuNP.

The extent of quenching observed for the different samples is difficult to rationalize probably because the pyrene groups on gold nanoparticles are subjected to multiple quenching effects such as the aggregation, the influence of the gold core, and the adsorption on the nanotube walls. In general, the interaction with nanotubes produces a greater quenching for nanoparticles than for **Pyr-SAc**, suggesting that the scarcely emissive pyrene units on the surface of the nanoparticles are more sensitive to the effects of adsorption on the SWCNTs. Assuming that some of the pyrene dyes on each nanoparticle (the ones on the opposite face) are not able to interact with the nanotube, a higher quenching efficiency for the nanoparticles with respect to **Pyr-SAc** would indicate that the pyrene units interacting with SWCNTs are almost not emissive. In this hypothesis, the observation of almost quantitative quenching of pyrene emission only for AuNP-100% could indicate that these nanoparticles interact simultaneously with more than one SWCNT (or SWCNT bundle), while mixed monolayer AuNPs appear to bind in a facial way just to a single nanotube (or bundle).

Preparation and Characterization of SWCNT−AuNP Nanohybrids. The results reported in the previous paragraph indicate that pyrene-functionalized AuNPs can interact with pristine SWCNTs. Such observation opens the way to the use of these two nanostructures to obtain self-organized nanohybrids.

To explore such a possibility, we applied a procedure based on consecutive centrifugation steps and aimed at isolating the water-soluble SWCNT−AuNP nanohybrids from water-soluble unbound AuNPs and insoluble SWCNTs, as illustrated in Figure 3.

Briefly, each sample of cofunctionalized AuNPs (2 mg) was mixed with pristine SWCNTs (1 mg) in water (5 mL), and the resulting suspension was sonicated at low power (1.2 W/mL) for 1 h. The resulting fine dispersion was expected to contain unbound AuNPs, the desired soluble SWCNT−AuNP nanohybrids, and insoluble SWCNTs (Figure 3a). Centrifugation of this mixture at low rounds removed the nonfunctionalized bundles of SWCNTs as a precipitate at the bottom of the centrifuge tube (Figure 3b). The supernatant was then submitted to several centrifugations at high rounds and resuspension cycles to separate the SWCNT−AuNP nanohybrids, which precipitate out from the suspension in this condition, from the unbound AuNPs that remain in the supernatant (Figure 3c). The absorption spectra of the supernatants collected from four subsequent washing steps, reported in Figure 4a, demonstrate the effectiveness of this purification stage. While cofunctionalized AuNPs were still present in the supernatant collected after the first washing, the intensity of their absorption spectrum decreases with subsequent washings until all the unbound AuNPs are removed.

Once purified, the SWCNT−AuNP nanohybrids were resuspended in water and characterized by TEM and spectroscopic measurements. In Figure 4b, we report the comparison between the absorption spectra of the cofunctionalized AuNP-5% and of the SWCNT−AuNP-5% nanohybrids. The latter present both the characteristic absorption bands of pyrene between 300 and 400 nm and the van Hove transitions of SWCNTs. While plasmonic contributions of SWCNTs and AuNPs overlap below 1000 nm and are hardly resolved, concentrations of nanotubes in solution could be estimated from the extinction coefficient for pristine SWCNTs at 1000

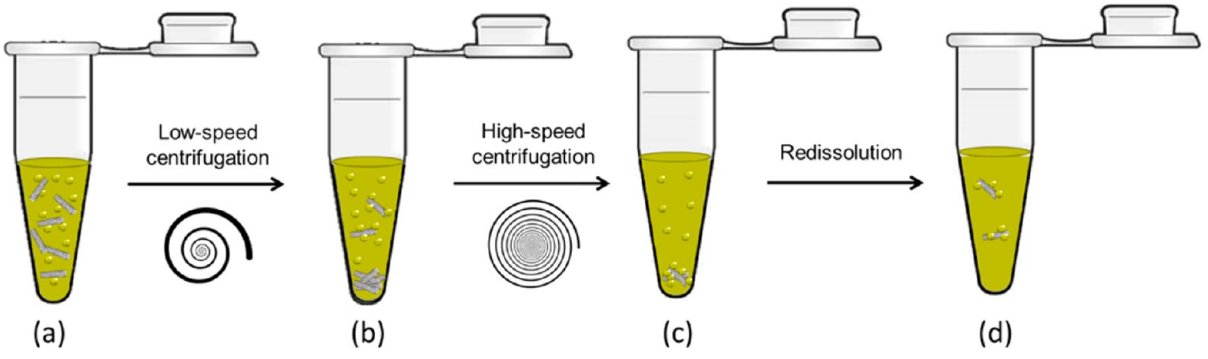

Figure 3. Representation of the process required to prepare the water-soluble SWCNT−AuNP nanohybrids: (a) sonication of a mixture of AuNPs and SWCNT in water to obtain a homogeneous dispersion; (b) removal of insoluble SWCNTs by low-speed centrifugation; (c) precipitation of the SWCNT−AuNP nanohybrids and removal of the free AuNPs in the supernatant by high-speed centrifugation; (d) redissolution of SWCNT−AuNP nanohybrids.

dx.doi.org/10.1021/jp505005e | J. Phys. Chem. C 2014, 118, 27028−27038

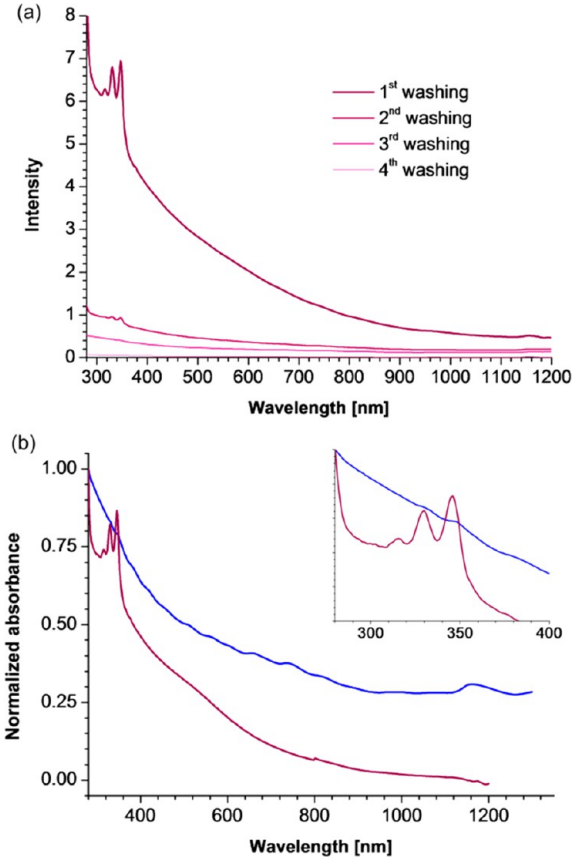

Figure 4. (a) Absorption spectra in Milli-Q water of the supernatants obtained from four subsequent washing steps in the preparation of SWCNT−AuNP-5% nanohybrids. (b) Absorption spectra of AuNP-5% (violet) and of the SWCNT−AuNP-5% nanohybrid in Milli-Q water. The inset highlights the absorption peaks of the pyrene units in the cofunctionalized AuNP-5% (violet) and in the SWCNT−AuNP-5% nanohybrid (blue).

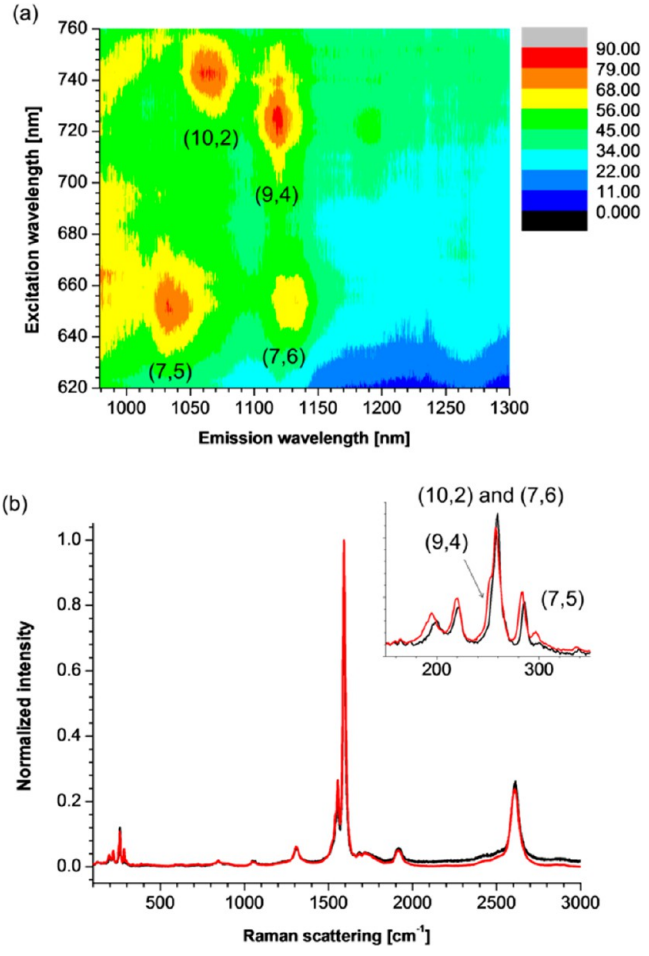

Figure 5. (a) Photoluminescence excitation maps of SWCNT−AuNP-5% nanohybrids in aqueous solution. (b) Raman spectra of the pristine SWCNTs (black) and of the SWCNT−AuNP-5% nanohybrids deposited on a glass substrate.

nm in DMF (9.8 ± 0.1 mL mg^{-1} cm^{-1}), assuming that it does not change upon interaction with the AuNPs in water.

All the mixed monolayer AuNPs were similarly effective in solubilizing pristine SWCNTs. In each case, concentrations ranging from 30 to 50 μg/mL were obtained, confirming the indication obtained by the fluorescence experiments that the affinity of the nanoparticles for the nanotubes is independent from the pyrene loading. On the other hand no CNTs were recovered when AuNP-0% was used.

At difference from what is observed in DMF, the aqueous solutions of each SWCNT−AuNP nanohybrid produced a barely detectable pyrene emission. Remarkably, the hybrids were instead emissive in the NIR region at wavelengths typical of the luminescence of semiconducting SWNTs. In Figure 5a we report the photoluminescence excitation map of SWCNT−AuNP-5% in aqueous solution.

As well-known, photoluminescence mapping allows us to correlate each luminescent peak with a specific subtype of SWCNTs identified by its chiral index.[40] On these bases we could ascertain the presence of (10,2)-, (9,4)-, (7,5)-, and (7,6)-SWCNTs from the analysis of the four luminescence peaks observed from the aqueous solution of the SWCNT−AuNP-5% nanohybrids. Moreover, the luminescence of these nanohybrids is an indication of the good degree of unbundling of SWCNTs promoted by cofunctionalized AuNPs and could provide the basis for photonics and imaging applications.

An analysis complementary to photoluminescence mapping is Raman spectroscopy. In the Raman spectrum of pristine SWCNTs (Figure 5b) the four typical SWCNT features are recognizable: (a) the G′-band at 2600 cm^{-1}, which is strongly dependent on perturbation of the phononic and/or electronic structures; (b) the G-band at 1600 cm^{-1} corresponding to the C−C stretching in graphite-like materials; (c) the D-band at 1300 cm^{-1}, which is correlated to the presence of disorder; and (d) the radial breathing mode (RBM) signals with diameter-dependent shifts between 200 and 300 cm^{-1}. Indeed, each of the SWCNT subtypes identified by photoluminescence mapping has a corresponding RBM signal. Interestingly, the comparison between the Raman spectra of pristine SWCNTs and the SWCNT−AuNP-5% nanohybrid does not highlight any changes in the distribution of RBM peaks. This result suggests that the interaction between the pyrene moieties in the cofunctionalized AuNPs and the CNT walls is not specific, while a selective interaction mediated by SWCNT electronic properties, and thus diameter-dependent, would have resulted in an enrichment of one or more SWCNT subtypes in solution. Remarkably, the noncovalent functionalization by the pyrene moieties does not introduce defects on the nanotube walls and hence preserves their structural integrity and electronic

dx.doi.org/10.1021/jp505005e | J. Phys. Chem. C 2014, 118, 27028−27038

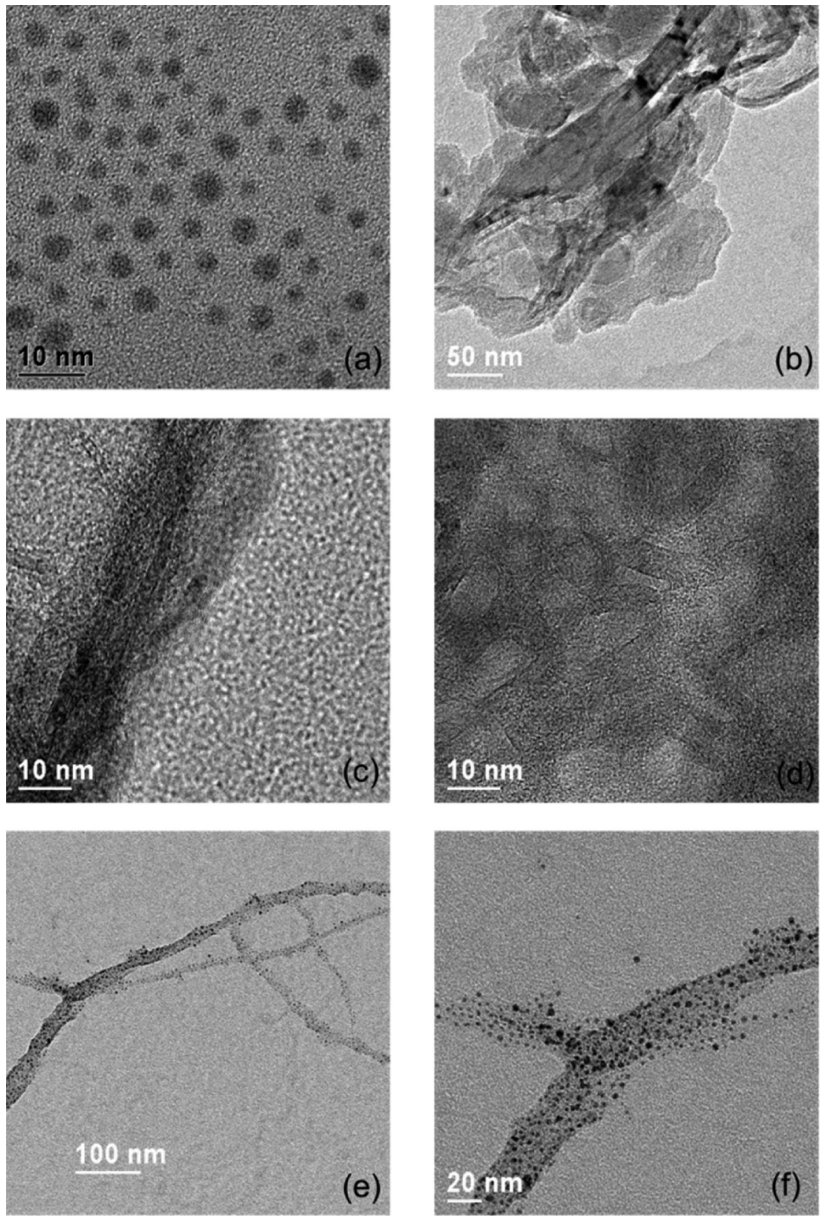

Figure 6. Preparation of SWCNT−AuNP nanohybrids. TEM images of samples obtained after the second centrifugation step (the one at high rounds) from (a) supernatant and (b, c) precipitate in the case of SWCNTs treated with AuNP-0% and from (d) supernatant and (e, f) precipitate in the case of SWCNTs treated with AuNP-5%.

properties. This is indicated by the observation that the D-band at 1300 cm^{-1}, which is ascribed to sp^3 defects on the nanotube walls,[41] is similar for SWCNT−AuNP-5% nanohybrids and pristine nanotubes.

To further corroborate these findings, we report in Figure 6 the TEM images of SWCNT−AuNP samples obtained from AuNP-0%, fully decorated with choline residues, and from cofunctionalized AuNP-5%. In the first case, AuNP-0% was found only in the supernatants from high speed centrifugation stages (a), while the final precipitate did not contain SWCNTs, but sparse carbon impurities (b, c). Arguably, AuNP-0% is unable to bind with the SWCNTs and to bring them in aqueous solution, and all the SWCNTs remain on the bottom of the centrifuge tube after the low-round centrifugation steps.

On the other hand, AuNPs with a mixed monolayer act as solubilizing agents toward SWCNTs since the pyrene moieties are able to bind to the SWCNT surface while the polar choline residues grant solubility in water. Indeed, after the low-round centrifugation step, part of the CNT material remains in solution together with the AuNP-5%. When this solution is centrifuged at the high speed round, all AuNP-5% and SWCNTs are collected at the bottom of the centrifuge tube (e, f), thus leaving supernatants clear of NPs (d).

The novel nanostructures we obtained are hybrids in which cofunctionalized AuNPs with diameter below 3 nm are homogeneously dispersed along the walls of small bundles of SWCNTs. Thanks to the robust interaction, the vast majority of the cofunctionalized AuNPs is bound to the SWCNT walls, even after the exhaustive washing stages.

■ CONCLUSIONS

In conclusion, we have herein demonstrated how it is possible to take multiple advantage of self-organization to obtain water-soluble SWCNT−AuNP nanohybrids. A small library of

dx.doi.org/10.1021/jp505005e | J. Phys. Chem. C 2014, 118, 27028−27038

multifunctional gold nanoparticles were easily prepared and screened for the ability to interact with pristine and functionalized carbon nanotubes and to provide them solubility in water. Interestingly enough, such ability does not depend on the amount of pyrene groups present at the nanoparticle surface. This indicates that the cooperation between pyrene units on the same nanoparticles in binding the nanotube walls is quite scarce. On the other hand, this also reveals that a very small amount of pyrene groups in the nanoparticle coating monolayer is required for binding. Consequently, the remaining surface is potentially available for the insertion of additional functional groups capable to empower the nanohybrid with more abilities. Indeed, the composition of the protecting monolayer of gold nanoparticles, as demonstrated here, can be easily modified by introducing different ligands and by varying their ratio. Hence, the use of cofunctionalized AuNPs to obtain soluble CNT derivatives with the desired properties offers potential advantages over different chemical modification approaches.

In addition, noncovalent functionalization does not spoil the electronic properties of the components, thus preserving, for example, CNT fluorescence in the NIR region. Moreover, we have provided a quantitative evaluation of the interaction in AuNP−CNT nanohybrids, which, to our knowledge, has not been previously detailed. Specifically, we have found that the association constant for complex formation of the pyrenyl residues depends on the composition of the AuNP monolayer and that this effect could be exploited to change the emissive properties of the nanohybrids.

AUTHOR INFORMATION

Corresponding Authors

*Fabrizio Mancin. E-mail: fabrizio.mancin@unipd.it. Phone: +39 049 827-5666.

*Enzo Menna. E-mail: enzo.menna@unipd.it. Phone: +39 049 827-5660.

Author Contributions

The manuscript was written through contributions of all authors. All authors have given approval to the final version of the manuscript.

Notes

The authors declare no competing financial interest.

ACKNOWLEDGMENTS

This work was supported by MIUR (grants FIRB-RBFR08DUX6, PRIN-20104XET32) and the ERC Starting Grant 2010 MOSAIC (259014).

REFERENCES

(1) Daniel, M.-C.; Astruc, D. Gold Nanoparticles: Assembly, Supramolecular Chemistry, Quantum-Size-Related Properties, and Applications toward Biology, Catalysis, and Nanotechnology. *Chem. Rev.* **2003**, *104*, 293−346.

(2) Scrimin, P.; Prins, L. J. Sensing through Signal Amplification. *Chem. Soc. Rev.* **2011**, *40*, 4488−4505.

(3) Haruta, M. When Gold Is Not Noble: Catalysis by Nanoparticles. *Chem. Rec.* **2003**, *3*, 75−87.

(4) Katz, E.; Willner, I. Integrated Nanoparticle−Biomolecule Hybrid Systems: Synthesis, Properties, and Applications. *Angew. Chem., Int. Ed.* **2004**, *43*, 6042−6108.

(5) Hutter, E.; Fendler, J. H. Exploitation of Localized Surface Plasmon Resonance. *Adv. Mater.* **2004**, *16*, 1685−1706.

(6) Giljohann, D. A.; Seferos, D. S.; Daniel, W. L.; Massich, M. D.; Patel, P. C.; Mirkin, C. A. Gold Nanoparticles for Biology and Medicine. *Angew. Chem., Int. Ed.* **2010**, *49*, 3280−3294.

(7) Schätz, A.; Reiser, O.; Stark, W. J. Nanoparticles as Semi-Heterogeneous Catalyst Supports. *Chem.—Eur. J.* **2010**, *16*, 8950−8967.

(8) Nie, Z.; Petukhova, A.; Kumacheva, E. Properties and Emerging Applications of Self-Assembled Structures Made from Inorganic Nanoparticles. *Nat. Nanotechnol.* **2010**, *5*, 15−25.

(9) Perrone, B.; Springhetti, S.; Ramadori, F.; Rastrelli, F.; Mancin, F. Nmr Chemosensing" Using Monolayer-Protected Nanoparticles as Receptors. *J. Am. Chem. Soc.* **2013**, *135*, 11768−11771.

(10) Diez-Castellnou, M.; Mancin, F.; Scrimin, P. Efficient Phosphodiester Cleaving Nanozymes Resulting from Multivalency and Local Medium Polarity Control. *J. Am. Chem. Soc.* **2014**, *136*, 1158−1161.

(11) Schnorr, J. M.; Swager, T. M. Emerging Applications of Carbon Nanotubes†. *Chem. Mater.* **2010**, *23*, 646−657.

(12) Gao, C.; Guo, Z.; Liu, J.-H.; Huang, X.-J. The New Age of Carbon Nanotubes: An Updated Review of Functionalized Carbon Nanotubes in Electrochemical Sensors. *Nanoscale* **2012**, *4*, 1948−1963.

(13) Cataldo, S.; Salice, P.; Menna, E.; Pignataro, B. Carbon Nanotubes and Organic Solar Cells. *Energy Environ. Sci.* **2012**, *5*, 5919−5940.

(14) Lu, R.; Christianson, C.; Kirkeminde, A.; Ren, S.; Wu, J. Extraordinary Photocurrent Harvesting at Type-Ii Heterojunction Interfaces: Toward High Detectivity Carbon Nanotube Infrared Detectors. *Nano Lett.* **2012**, 6244−6249.

(15) Lamanna, G.; Battigelli, A.; Ménard-Moyon, C.; Bianco, A. Multifunctionalized Carbon Nanotubes as Advanced Multimodal Nanomaterials for Biomedical Applications. *Nanotechnology Reviews* **2012**, *1*, 17.

(16) Chen, G. Z.; Shaffer, M. S. P.; Coleby, D.; Dixon, G.; Zhou, W.; Fray, D. J.; Windle, A. H. Carbon Nanotube and Polypyrrole Composites: Coating and Doping. *Adv. Mater.* **2000**, *12*, 522−526.

(17) Wildgoose, G. G.; Banks, C. E.; Compton, R. G. Metal Nanoparticles and Related Materials Supported on Carbon Nanotubes: Methods and Applications. *Small* **2006**, *2*, 182−193.

(18) Saito, Y. *Carbon Nanotube and Related Field Emitters: Fundamentals and Applications*; Wiley-VCH: Weinheim, 2010; p 504.

(19) Quinn, B. M.; Dekker, C.; Lemay, S. G. Electrodeposition of Noble Metal Nanoparticles on Carbon Nanotubes. *J. Am. Chem. Soc.* **2005**, *127*, 6146−6147.

(20) Chopra, N.; Majumder, M.; Hinds, B. J. Bifunctional Carbon Nanotubes by Sidewall Protection. *Adv. Funct. Mater.* **2005**, *15*, 858−864.

(21) Ismaili, H.; Lagugné-Labarthet, F. o.; Workentin, M. S. Covalently Assembled Gold Nanoparticle-Carbon Nanotube Hybrids Via a Photoinitiated Carbene Addition Reaction. *Chem. Mater.* **2011**, *23*, 1519−1525.

(22) Guldi, D. M.; Menna, E.; Maggini, M.; Marcaccio, M.; Paolucci, D.; Paolucci, F.; Campidelli, S.; Prato, M.; Rahman, G. M. A.; Schergna, S. Supramolecular Hybrids of [60]Fullerene and Single-Wall Carbon Nanotubes. *Chem.—Eur. J.* **2006**, *12*, 3975−3983.

(23) Tran, P. D.; Le Goff, A.; Heidkamp, J.; Jousselme, B.; Guillet, N.; Palacin, S.; Dau, H.; Fontecave, M.; Artero, V. Noncovalent Modification of Carbon Nanotubes with Pyrene-Functionalized Nickel Complexes: Carbon Monoxide Tolerant Catalysts for Hydrogen Evolution and Uptake. *Angew. Chem., Int. Ed.* **2011**, *50*, 1371−1374.

(24) Majeed, S.; Filiz, V.; Shishatskiy, S.; Wind, J.; Abetz, C.; Abetz, V. Pyrene-Poss Nanohybrid as a Dispersant for Carbon Nanotubes in Solvents of Various Polarities: Its Synthesis and Application in the Preparation of a Composite Membrane. *Nanoscale Res. Lett.* **2012**, *7*, 1−11.

(25) Haddad, R.; Holzinger, M.; Maaref, A.; Cosnier, S. Pyrene Functionalized Single-Walled Carbon Nanotubes as Precursors for High Performance Biosensors. *Electrochim. Acta* **2010**, *55*, 7800−7803.

(26) Liu, L.; Wang, T.; Li, J.; Guo, Z.-X.; Dai, L.; Zhang, D.; Zhu, D. Self-Assembly of Gold Nanoparticles to Carbon Nanotubes Using a Thiol-Terminated Pyrene as Interlinker. *Chem. Phys. Lett.* **2003**, *367*, 747−752.
(27) Holmlin, R. E.; Chen, X.; Chapman, R. G.; Takayama, S.; Whitesides, G. M. Zwitterionic Sams That Resist Nonspecific Adsorption of Protein from Aqueous Buffer. *Langmuir* **2001**, *17*, 2841−2850.
(28) Manea, F.; Bindoli, C.; Polizzi, S.; Lay, L.; Scrimin, P. Expeditious Synthesis of Water-Soluble, Monolayer-Protected Gold Nanoparticles of Controlled Size and Monolayer Composition. *Langmuir* **2008**, *24*, 4120−4124.
(29) Pengo, P.; Polizzi, S.; Battagliarin, M.; Pasquato, L.; Scrimin, P. Synthesis, Characterization and Properties of Water-Soluble Gold Nanoparticles with Tunable Core Size. *J. Mater. Chem.* **2003**, *13*, 2471−2478.
(30) Jana, N. R.; Peng, X. Single-Phase and Gram-Scale Routes toward Nearly Monodisperse Au and Other Noble Metal Nanocrystals. *J. Am. Chem. Soc.* **2003**, *125*, 14280−14281.
(31) Guarino, G.; Rastrelli, F.; Scrimin, P.; Mancin, F. Lanthanide-Based Nmr: A Tool to Investigate Component Distribution in Mixed-Monolayer-Protected Nanoparticles. *J. Am. Chem. Soc.* **2012**, *134*, 7200−7203.
(32) Battistini, G.; Cozzi, P. G.; Jalkanen, J.-P.; Montalti, M.; Prodi, L.; Zaccheroni, N.; Zerbetto, F. The Erratic Emission of Pyrene on Gold Nanoparticles. *ACS Nano* **2008**, *2*, 77−84.
(33) Montalti, M.; Prodi, L.; Zaccheroni, N.; Battistini, G. Modulation of the Photophysical Properties of Gold Nanoparticles by Accurate Control of the Surface Coverage. *Langmuir* **2004**, *20*, 7884−7886.
(34) Georgakilas, V.; Gournis, D.; Tzitzios, V.; Pasquato, L.; Guldi, D. M.; Prato, M. Decorating Carbon Nanotubes with Metal or Semiconductor Nanoparticles. *J. Mater. Chem.* **2007**, *17*, 2679−2694.
(35) Zhao, Y. L.; Stoddart, J. F. Noncovalent Functionalization of Single-Walled Carbon Nanotubes. *Acc. Chem. Res.* **2009**, *42*, 1161−1171.
(36) Britz, D. A.; Khlobystov, A. N. Noncovalent Interactions of Molecules with Single Walled Carbon Nanotubes. *Chem. Soc. Rev.* **2006**, *35*, 637−659.
(37) Ahmad, A.; Kurkina, T.; Kern, K.; Balasubramanian, K. Applications of the Static Quenching of Rhodamine B by Carbon Nanotubes. *ChemPhysChem* **2009**, *10*, 2251−2255.
(38) D'Este, M.; De Nardi, M.; Menna, E. A Co-Functionalization Approach to Soluble and Functional Single-Walled Carbon Nanotubes. *Eur. J. Org. Chem.* **2006**, *2006*, 2517−2522.
(39) Menna, E.; Scorrano, G.; Maggini, M.; Cavallaro, M.; Della Negra, F.; Battagliarin, M.; Bozio, R.; Fantinel, F.; Meneghetti, M. Shortened Single-Walled Nanotubes Functionalized with Poly (Ethylene Glycol): Preparation and Properties. *Arkivoc* **2003**, *12*, 64−73.
(40) Bachilo, S. M.; Strano, M. S.; Kittrell, C.; Hauge, R. H.; Smalley, R. E.; Weisman, R. B. Structure-Assigned Optical Spectra of Single-Walled Carbon Nanotubes. *Science* **2002**, *298*, 2361−2366.
(41) Graupner, R. Raman Spectroscopy of Covalently Functionalized Single-Wall Carbon Nanotubes. *J. Raman Spectrosc.* **2007**, *38*, 673−683.